Petrophysical environment of sediments hosting gas hydrate, JAPEX/JNOC/GSC Mallik 2L-38 gas hydrate research well

T.J. Katsube[1], S.R. Dallimore[1], T. Uchida[2], K.A. Jenner[3], T.S. Collett[4], and S. Connell[1]

Abstract: A petrophysical study has been performed on mudstone and sandstone samples from depths of 880–950 m to determine the petrophysical controls on gas hydrate distribution in the sedimentary sequence at the JAPEX/JNOC/GSC Mallik 2L-38 well site, Northwest Territories, Canada. Within the cored interval of the Mallik 2L-38 well gas hydrate is hosted in two sandstone horizons with overlying and underlying mudstone horizons, with minor gas hydrate concentrations within some mudstone formations.

Results indicate that, although the interbedded mudstone units have relatively high porosities (24–30%) and are at relatively shallow depths, they have a well developed framework-supported texture, probably due to high silt and sand content (56–78 weight per cent), and a maximum burial depth greater than present. Regardless of this, the minor matrix content (13–25 weight per cent) controls the fluid transport characteristics, resulting in extremely low mudstone permeability sections (2×10^{-21} m to 2×10^{-19} m^2). There are indications that these low permeabilities and the storage pore sizes contribute to the gas hydrate distribution.

Résumé : Une étude pétrophysique a été effectuée sur les échantillons de mudstones et de grès prélevés à des profondeurs de 880 à 950 m afin de déterminer les facteurs pétrophysiques qui contrôlent la répartition des hydrates de gaz dans la séquence sédimentaire à l'emplacement du puits JAPEX/JNOC/GSC Mallik 2L-38 (Territoires du Nord-Ouest, Canada). Dans l'intervalle carotté du puits Mallik 2L-38, des hydrates de gaz sont présents dans deux horizons de grès encadrés vers le haut et vers le bas par des horizons de mud-stone. Certaines formations de mudstone contiennent des concentrations mineures d'hydrates de gaz.

Les résultats indiquent que bien que les unités de mudstone interstratifiées se rencontrent à des profondeurs relativement faibles et que leur porosité soit relativement élevée (de 24 à 30 %), les mudstones montrent une texture jointive bien développée, probablement en raison de leur forte teneur en silt et en sable (de 56 à 78 % en poids), et rendent compte d'une profondeur d'enfouissement maximale supérieure à la profondeur actuelle. Malgré cela, la matrice peu importante des mudstones (de 13 à 25 % en poids) contrôle les caractéristiques de la circulation des fluides, ce qui engendre des valeurs de perméabilité extrêmement faibles (de 2×10^{-21} à 2×10^{-19} m^2) dans les sections occupées par ceux-ci. Ces faibles valeurs de perméabilité et la taille des pores de stockage auraient une incidence sur la répartition des hydrates de gaz.

[1] Geological Survey of Canada, 601 Booth Street, Ottawa, Ontario, Canada K1A 0E8
[2] JAPEX Research Centre, Japan Petroleum Exploration Company, Ltd., 1-2-1 Hamada, Mihama-ku, Chiba 261-0025 Japan
[3] Geological Survey of Canada (Atlantic), P.O. Box 1006, Dartmouth, Nova Scotia, Canada B2Y 4A2
[4] United States Geological Survey, Denver Federal Center, Box 25046, MS-939, Denver, Colorado 80225, U.S.A.

INTRODUCTION

A petrophysical study has been performed on a suite of mudstone and sandstone samples from depths of 880–950 m in order to determine the petrophysical environment of the gas-hydrate-bearing sedimentary sequence at the Mallik 2L-38 well site, Northwest Territories, Canada. The main gas hydrate in the cored interval at this site is hosted in two sandstone units, at depths of 896–924 m and 950–1005 m (all depths were measured from kelly bushing [8.31 m above sea level]), (Fig. 1) with overlying and underlying units. There is a minor concentration of gas hydrate within the mudstone at the 934–944 m interval (Fig. 1). The main question is what are the petrophysical controls over the gas hydrate distribution. The fact that they are hosted not only in sandstone but also in some mudstone horizons is of considerable interest. A related question is whether these mudstone horizons contained a seal that could have acted as a trap for hydrocarbons prior to or during glaciation. In an attempt to find answers to these questions, this study analyzes the results of porosity, pore-size distribution, mudstone texture, low permeability, and

pore-structure evolution (Katsube, 1999; T.J. Katsube, T. Uchida, S.R Dallimore, K.A., Jenner, T.S. Collett, and S. Connell, unpub. manuscript, 1999; K. Coyner, T.J. Katsube, and S.R. Dallimore, unpub. manuscript, 1999; G.N. Boitnott, T.J. Katsube, S. Connell, and S.R. Dallimore, unpub. manuscript, 1999) studies carried out on samples collected from the Mallik 2L-38 well site.

Natural gas hydrate is a solid substance formed from natural gas and water which can occur within sediments in association with deep permafrost and in marine settings. While a considerable body of knowledge is available on the physical characteristics of bulk gas hydrate, much less is known about its properties when it is present within naturally occurring sediments. In addition to the in situ pressure and temperature regime characteristic of a particular geological environment, the stability of gas hydrate is thought to be controlled by the chemistry of the pore fluids and fundamental porous media properties such as mineralogy, porosity, permeability, and pore-size distribution. Given that the majority of gas hydrate deposits in nature occur within the pore spaces, the porous media properties are also likely to exert primary controls on
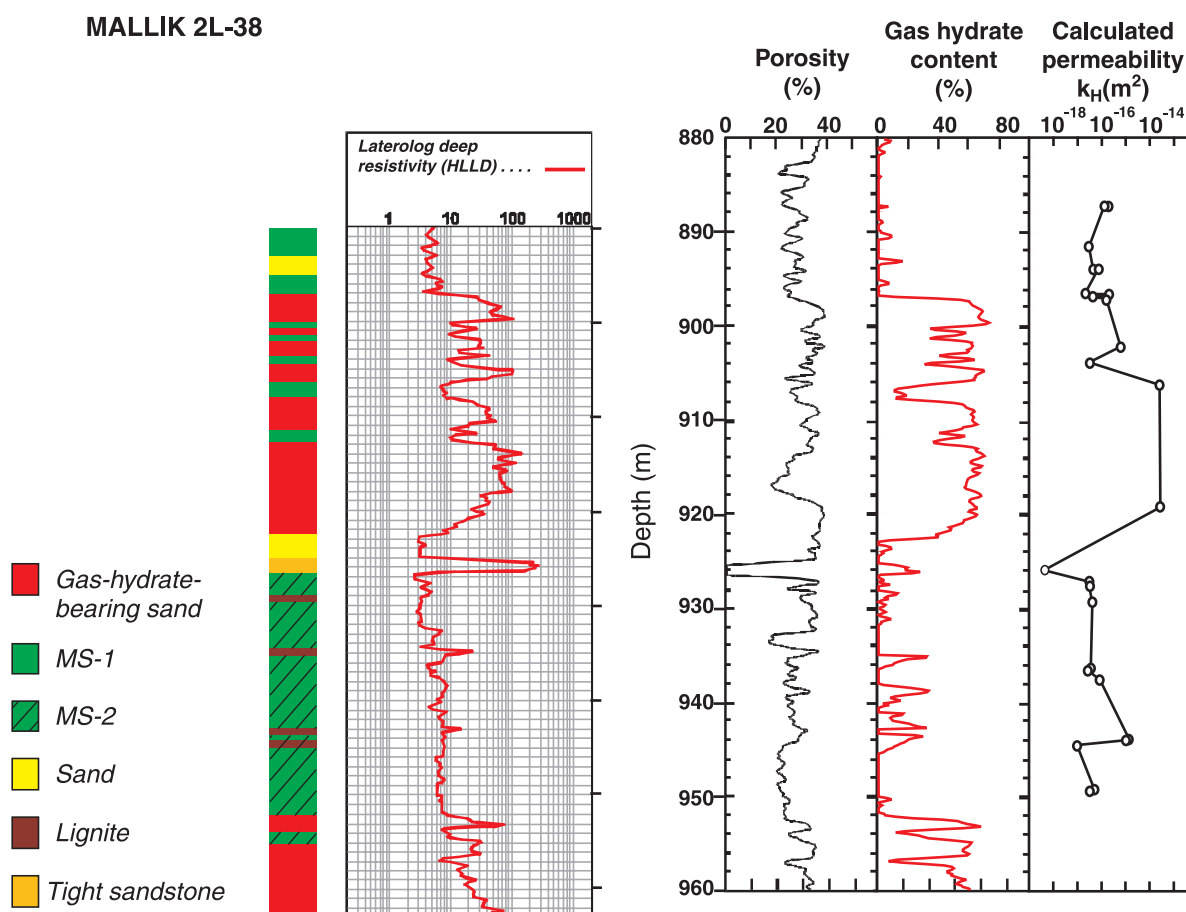

Figure 1. *Lithological units (Jenner et al., 1999), geophysical logs (Formation resistivity, porosity, gas hydrate content from Collett et al., 1999) and calculated high permeabilities (k_H, T.J. Katsube, T. Uchida, S.R Dallimore, K.A., Jenner, T.S. Collett, and S. Connell, unpub. manuscript, 1999) For the formations hosting the gas hydrate at the Mallik 2L-38 well site, Northwest Territories, Canada. Units MS-1 and MS-2 represent the two mudstone (silt, sandy silt, clayey silt) sequences.*

the volume of gas hydrate which can occur within particular sediments. These fundamental physical properties are critical inputs in production simulation models as they exert primary controls over fluid and gas flow.

The Mallik 2L-38 research well provided a unique opportunity to conduct fundamental geological, geochemical, and geophysical studies of core samples from a permafrost-hosted gas hydrate occurrence. As part of an integrated suite of laboratory studies, this paper presents the results of detailed petrophysical studies on core samples from the gas-hydrate-bearing interval between 890 m and 952 m. These results consist of petrophysical (e.g. pore structure, permeability, and porosity), textural, and mineralogical data of the mudstone and sandstone samples from the well site, obtained by a variety of special and conventional techniques; the implications of the results are also discussed.

GEOLOGY

Detailed studies of the cored interval from 886 m to 952.6 m combined with quantitative well-log analyses have revealed a complex sedimentary succession with variable sedimentology (Jenner et al., 1999) and associated gas hydrate concentrations. These are Oligocene to Holocene sediments comprised of three (Kugmallit, Mackenzie Bay, and Iperk sequences) of the eleven transgressive-regressive sequences proposed by Dixon et al. (1992). As illustrated in Figure 1, the main gas hydrate body at 896 m is overlain by poorly consolidated mudstone with minor sandstone interbeds. Between 896 m and 926 m the sediments (Mackenzie Bay Sequence) consist of unconsolidated, medium-grained sandstone with minor interbeds of poorly consolidated mudstone. Well-log estimates suggest that the sandstone contains high in situ gas hydrate concentrations occupying between 30% and 80% of the pore space (Collett et al., 1999; Miyairi et al., 1999). Mudstone interbeds have lower concentrations between 20% and 60%. Core samples in this interval were frozen when retrieved as a consequence of endothermic cooling from gas hydrate dissociation during transit of the core to the surface (Wright et al., 1999). Most of the gas hydrate observed or detected immediately after recovery occurred within the pore spaces of the sandstone. However, a variety of visible gas hydrate forms were also observed. The base of the sandstone interval included a thin zone with no gas hydrate and a very distinct dolomite-cemented sandstone from the 925–926 m depth. This cemented sandstone is identified by high resistivity and very low porosity peaks in the geophysical logs (Fig. 1). From 926 m to the base of the cored interval at 950 m, the sediments (Kugmallit Sequence) were composed of poorly consolidated mudstone with well-log-inferred gas hydrate concentrations between 0 and 40%. No visible evidence of gas hydrate was observed in the core samples. Below 950 m, well-log data suggests another sandstone sequence occurs with high gas hydrate concentrations similar to the zone from 896 m to 925 m.

The core samples used in this study were collected with a conventional core barrel which recovered either 15 cm or 10 cm diameter core samples (Ohara et al., 1999).

Subsamples for petrophysical studies were taken of intact pristine core samples after gas hydrate dissociation. Samples were kept frozen until testing. The porosity analyses were conducted on irregularly shaped specimens of 1–3 cm³ in volume, which were cut from these subsamples. Irregular-shaped specimens showing good cross-sections of the lithology were selected for the mudstone texture analysis, which consists of thin-section analyses, scanning electron microscopy (SEM), and X-ray diffraction analyses (XRD). Several disc specimens, each 2.5 cm in diameter and 0.5–1.5 cm in thickness, were also cored from the subsamples to determine the pressure characteristics of the permeability and storage and/or connecting pores. In total, a suite of 22 samples consisting of unconsolidated sandstone, cemented sandstone, and mudstone were analyzed (sample numbers EJA-1 to EJA-22).

The geological and geophysical logs (Collett et al., 1999) were used to identify four lithological units of interest to this study (Fig. 1): gas-hydrate-bearing sandstone, barren sandstone, tight sandstone, and mudstone. 'Mudstone' in this paper implies units consisting of silt, sandy silt, and clayey silt. There are two gas-hydrate-bearing sandstone formations, an upper (formation GH-SS-1) and a lower (formation GH-SS-2). Of particular interest are two mudstone subunits, MS-1 (895–925 m) and MS-2 (926.5–952 m).

BASIC POROSITY CONCEPTS

The character of the pore structure within a particular sediment is a consequence of the mineralogy and packing imposed during deposition and the history of compaction and diagenesis which the sediment has undergone subsequent to deposition. For coarse-grained sediments such as sandstone, pore structure is largely controlled by grain-to-grain contacts and the nature and degree of cementation. The pore-size distribution of finer grained sediments such as mudstone is more complex. Two pore-structure models are frequently used to explain petrophysical characteristics of mudstone (Katsube and Williamson, 1994; Katsube et al., 1997). Figures 2a and 2b describe the 'Storage–connecting-pore model' and the 'Pore-size distribution model', respectively. The latter consists of a bundle of tubular pores with different diameters. The former explains the basic pore-shape and grain-shape relationship of pores in sedimentary rocks and the latter displays the size distribution of these pores; essentially both explain different aspects of the same pores. Storage and connecting pores (Fig. 2a) are two major components of these pore-structure models. Using these models, fluid-flow paths can be considered in terms of connecting pores and parts of the storage pores, usually represented by pore sizes in the vicinity of the mode (Katsube et al., 1992; Katsube and Williamson, 1994, 1998). Recent studies have also shown that the pore-size distribution patterns can be used to provide information on mudstone texture and other petrophysical characteristics, such as degree of compaction (e.g. Katsube and Williamson, 1994, 1998; Katsube et al., 1995). It is also possible to make permeability estimates from these distribution patterns (e.g. Uchida, 1987; Katsube et al., 1998; Katsube and Connell, 1998).
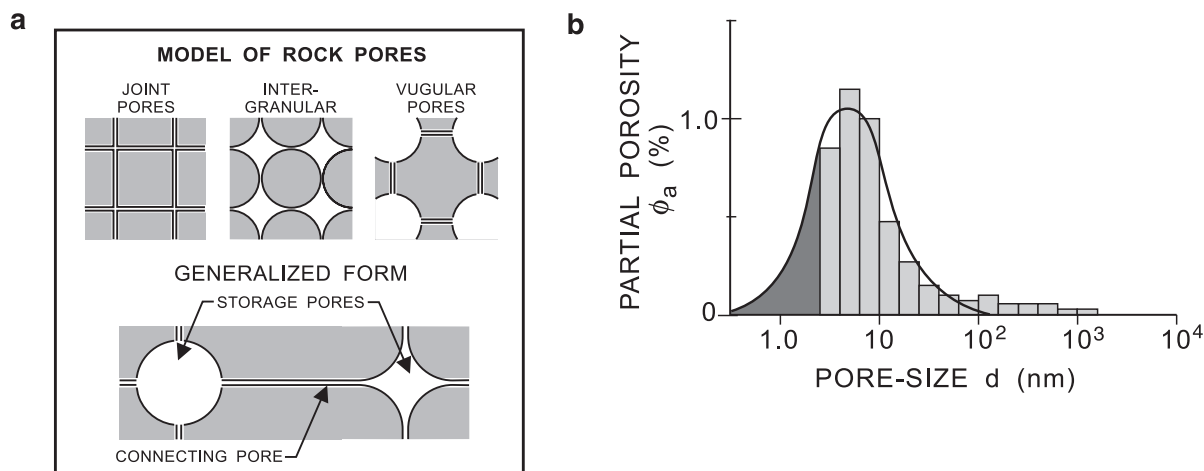
a

b

Figure 2. Pore structure models used for characterizing mudstones (Katsube and Williamson, 1994, 1998) **a)** *Storage-connecting pore model (Katsube and Collett, 1975), and* **b)** *pore-size distribution model (Katsube, 1992). The ø$_a$ is partial porosity, and 'd' is the general expression for pore sizes.*

Table 1. Standard porosity and pore-size distribution data for the sandstone (SS), including the tight cemented sandstone (T-SS), and the mudstone (MS) samples collected from the Mallik 2L-38 well site, Northwest Territories, Canada.

Sample	Fm	h (m)	ϕ_E (%)	ϕ_{rr} (%)	ϕ_s (%)	ϕ_c (%)	ϕ_{np} (%)	ϕ_{ip} (%)	ϕ_{mp} (%)	$\phi_{ip}+\phi_{mp}$ (%)
EJA-1	MS	896.8	25.7	0.63	13.7	8.17	4.57	17.3	2.69	20.0
		896.8	29.5	–	–	–	–	–	–	–
EJA-2	MS	896.4	27	0.44	11.7	14.5	6.96	19.2	2.88	22.0
		896.4	29.5	–	–	–	–	–	–	–
EJA-3	MS	887.3	28.9	0.79	15.9	4.22	3.39	16.8	4.85	21.6
EJA-4	MS	897.1	28.3	0.88	16.8	2.39	4.04	15.1	4.77	19.8
EJA-5	SS	906.2	35.5	0.92	32.7	2.84	2.33	3.72	29.5	33.2
EJA-6	SS	919.1	36.4	0.83	30.2	6.20	2.79	1.80	31.8	33.6
EJA-7	T-SS	925.9	2.2	0.33	0.65	1.31	1.61	0.35	0.25	0.58
EJA-8	MS	927.6	24.3	0.64	14.4	8.10	4.22	18.2	3.39	21.6
EJA-9	MS**	949.4	25.4	0.56	13.8	10.7	6.01	18.5	2.83	21.4
EJA-10	MS	897.1	27.7	0.77	16.3	4.91	–	–	–	–
EJA-11	SS	893.9	23.8	0.53	14.0	12.6	3.97	22.7	–	24.1
EJA-13	MS	903.9	28.6	0.56	17.2	13.6	5.82	24.9	–	27.7
EJA-14	MS**	936.7	24.2	0.49	12.9	13.6	4.68	21.9	–	23.7
EJA-15	MS	944.5	22.7	0.35	8.7	16.1	6.0	18.8	–	19.8
EJA-16	MS	887.3	29.4	–	–	–	–	–	–	–
EJA-17	MS	927.6	30.3	–	–	–	–	–	–	–
EJA-18	MS	949.4	26.1	–	–	–	–	–	–	–
EJA-19	MS	949.4	26.2	–	–	–	–	–	–	–
EJA-20A	MS	896.7	26.3	–	–	–	–	–	–	–
EJA-20B	MS	896.7	–	0.74	14.6	5.08	3.77	16.0	–	18.1
EJA-21	MS	928.3	27.3	–	–	–	–	–	–	–
EJA-22	MS	928.6	25.6	–	–	–	–	–	–	–

Fm	=	Formation
**	=	Bioturbated (Jenner et al., 1999)
h	=	Depth
ϕ_E	=	Effective porosity (represented by the helium porosity)
ϕ_{rr}	=	Storage porosity ratio
ϕ_S	=	Storage porosity
ϕ_C	=	Connecting porosity
ϕ_{np}	=	Nano-pore Porosity (2.5–25 nm)
ϕ_{ip}	=	Intermediate-pore Porosity (25 nm to 10 µm)
ϕ_{mp}	=	Micro-pore Porosity (10–250 µm)
–	=	No data

A summary published previously (Katsube and Williamson, 1994, 1998) on pore-structure parameters used to characterize mudstone is repeated in part here. Among these parameters are effective porosity, ϕ_E; partial porosity, ϕ_a; storage porosity ratio, ϕ_{rr}; and pore surface area, A. The ϕ_E, in principle, represents the pore space in all interconnected pores, and is expressed by (Katsube et al., 1997)

$$\phi_E = \phi_s + \phi_c, \tag{1}$$

where ϕ_s and ϕ_c are the porosities of the storage and connecting pores, respectively. The display format used for the pore-size distribution, d (Fig. 2b), has each decade of the logarithmic pore-size scale (x-axis) subdivided into five ranges with equal physical spacing (Katsube and Issler, 1993). The porosity contained in each pore-size range is represented by ϕ_a. The sum of ϕ_a for all pore sizes is represented by ϕ_{Hg} which is, in principal, equal to ϕ_E. The ϕ_{rr} is represented by (Katsube et al., 1997)

$$\phi_{rr} = \phi_s / \phi_E. \tag{2}$$

Pore surface area (A), in this case, is the sum of the pore surface area of all pore sizes represented by cylindrical tubes of varied diameters and length, and can be expressed by

$$A = \sum_{i=1}^{n} \left[4\phi_{ai} / (d_{ai}\delta_{BD}) \right], \tag{3}$$

where ϕ_{ai} and d_{ai} are the partial porosity and geometric mean pore size for the i-th pore-size range, and δ_{BD} is the bulk density.

Helium (Loman et al., 1993) and mercury porosimetry (Washburn, 1921; Rootare, 1970; Katsube and Issler, 1993) have been used to determine the porosity and pore-size distribution in this study. Although ϕ_E can also be determined by the latter method, as previously indicated, helium porosimetry is actually chosen for representation, in this case, because mercury porosimetry does not include the pore space in pores smaller than 2.5 nm (Katsube et al., 1997). The storage porosity ratio (ϕ_{rr}) is determined by taking the ratio of the total mercury residual volume following extrusion over the total mercury intrusion volume (Appendix Fig. A1) using mercury porosimetry (Katsube et al., 1997). Using these ϕ_E and ϕ_{rr} values, ϕ_s and ϕ_c are derived by the following equations:

$$\phi_s = \phi_{rr}\phi_{Hg} \tag{4}$$

$$\phi_c = \phi_{Hg} - \phi_s. \tag{5}$$

PORE-STRUCTURE CHARACTERISTICS

The results of a pore-structure study consisting of mercury porosimetry, helium porosimetry, and grain-size analysis (laser particle-size analysis) carried out on a suite of mudstone and sandstone samples from the Mallik 2L-38 well site (T.J. Katsube, T. Uchida, S.R Dallimore, K.A., Jenner, T.S. Collett, and S. Connell, unpub. manuscript, 1999) are listed in Tables 1 to 3. Table 3 contains some data obtained from other work (Uchida et al., 1999). The effective porosity

Table 2. Grain-size (particle-size distribution) data for the nine sandstone (SS) and mudstone (MS) samples collected from the Mallik 2L-38 well site.

Sample	Fm	h (m)	Cly (wt %)	Slt (wt %)	Snd (wt %)
EJA-1	MS	896.8	17.2	72.4	10.4
EJA-2	MS	896.4	13.2	57.0	29.8
EJA-3	MS	887.3	14.2	55.7	25.4
EJA-4	MS	897.1	12.9	58.2	23.6
EJA-5	SS	906.2	6.8	33.3	59.9
EJA-6	SS	919.1	0	8.3	91.7
EJA-7	T-SS	925.9	6.4	45.0	48.6
EJA-8	MS	927.6	24.8	75.6	0.8
EJA-9	MS	949.4	22.0	78.0	0

Fm	=	Formation
T-SS	=	Tight cemented sandstone
h	=	Depth
Cly	=	Clay
Slt	=	Silt content
Snd	=	Sand content

Table 3. Calculated permeability values, using the following equation constrained for low permeability rocks (Katsube et al., 1998):

$$k_L = 1 \times 10^{-21} \exp(0.13 d_1 - 0.68), \tag{6}$$

and for higher permeability rocks (Uchida, 1987):

$$k_H = 0.62 \text{Log} \left[\phi_{Hg}(d_{MD}/2)^2 / A \right] + 0.675. \tag{7}$$

Depth h (m)	ϕ_{Hg} (%)	A (m^2/g)	d_1 (nm)	d_{MD} (mm)	k_L (x$10^{-21}m^2$)	k_H (x$10^{-18}m^2$)	
887.2	37.5	5.2	–	0.56	–	191	U
887.3	25.0	10.9	5.0	0.74	0.97	132	
891.5	28.0	7.8	–	0.18	–	30.4	U
893.9	28.1	11.1	5.0	0.31	0.97	47.3	
894.0	30.4	6.8	–	0.34	–	76.6	U
896.4	29.0	20.9	5.0	0.21	0.97	20.9	
896.5	31.1	5.0	–	0.62	–	199	U
896.8	24.6	14.8	5.0	0.36	0.97	43.7	
897.1	23.8	14.2	5.0	0.98	0.97	155	
902.2	32.9	4.6	–	1.42	–	603	U
903.9	33.5	18.1	5.0	0.27	0.97	32.8	
906.2	42.4	13.9	–	44.00	–	2510	
919.1	47.4	14.4	–	44.00	–	2630	
925.9	2.19	3.7	5.0	0.014	0.97	0.431	
927.0	26.8	8.8	–	0.20	–	31.3	U
927.6	25.8	14.0	7.9	0.27	1.41	33.0	
929.2	27.4	9.1	–	0.26	–	43.0	U
936.3	25.2	6.9	–	0.20	–	35.0	U
936.7	28.4	13.1	5.0	0.22	0.97	27.7	
937.5	28.1	7.0	–	0.38	–	82.2	U
943.8	24.8	24.6	–	7.24	–	135	U
944.1	20.4	29.5	–	6.98	–	102	U
944.5	25.8	16.6	5.0	0.11	0.97	9.48	
949.1	25.3	6.8	–	0.26	–	49.0	U
949.4	27.4	20.4	5.0	0.30	0.97	32.0	

U	=	Additional data from another source (Uchida et al., 1999)
ϕ_{Hg}	=	Effective porosity determined by mercury porosimetry for the pore-size range of 2.5 nm to 250 μm, respectively
A	=	Pore surface areas determined by mercury porosimetry (Uchida et al., 1999; T.J. Katsube, T. Uchida, S.R. Dallimore, K.A. Jenner, T.S. Collett, and S. Connell, unpub. manuscript, 1999).
d_1	=	First mode of the pore-size distribution
d_{MD}	=	Median pore-size (Determined by a method similar to d_G, Uchida, 1987)
–	=	No data

(ϕ_E), storage porosity (ϕ_s) and connecting porosity (ϕ_C) are in the ranges of 24–36%, 11.7 to more than 30%, and 2.4–14.5%, respectively for the sandstone and mudstone samples used in this study, except for a well cemented sandstone (sample T-SS: ϕ_E=2.2%, ϕ_s=0.65%, and =ϕ_c 1.31%). The silt, clay, and sand contents of the mudstone samples are in the ranges of 56–78%, 13–25%, and 0–30%, respectively, indicating the dominance of silt.

The pore-size distributions for 14 of the sandstone and mudstone samples from the Mallik 2L-38 well site are displayed in Figures 3–6. The pore-size distribution for the two unconsolidated sandstone samples (EJA-5, EJA-6) and the cemented sandstone (sample EJA-7) are displayed in Figure 3. The logarithmic scale is used for the vertical axis to enhance the smaller partial porosities (ϕ_a) of the nano-pores (2.5–40 nm). This figure shows that the distribution patterns are generally similar for the two unconsolidated sandstone samples (Fig. 3a, b), but their large partial porosities (ϕ_a) in the larger pore-size range (40–160 µm) disappear for the cemented sandstone (Fig. 3c). The pore-size distributions for the seven samples in mudstone unit 1 (MS-1) and the four samples in mudstone unit 2 (MS-2) are displayed in Figures 4 and 5, respectively. While the partial porosity (ϕ_a) values for the modes vary, the pore-size distribution patterns are generally similar for these two units. However, the ϕ_a values are

smaller in the 1–16 µm range for MS-2 samples compared to MS-1 samples. The pore-size distributions for these three rock types: unconsolidated sandstone, cemented sandstone, and mudstone can be characterized by the examples displayed in Figure 6a–c. The average pore-size distribution (Fig. 6d) of these samples displays a trimodal distribution pattern. Following a statistical analysis technique previously applied for analysis of the pore-size distribution (Agterberg et al., 1984), this average pore-size distribution is used to determine the pore sizes that separate the three porosity groups, nano-pore porosities (ϕ_{np}: d=2.5–25 nm), intermediate pore porosities (ϕ_{ip}: d=25 nm to 10 µm) and micro-pore porosities (ϕ_{mp}: d=10–250 µm), with corresponding modes of d_1, d_2, and d_3, respectively. The parameter 'd' represents the ranges of the pore-size distribution. Figure 6a (sample EJA-6) displays a pore-size distribution pattern dominated by ϕ_{mp} (d=10–250 µm) with a major mode (d_3) value of 50 µm, typical of a sandstone. The pore-size distribution pattern dominated by ϕ_{np} (d=2.5–25 nm) with a major mode (d_1) value of 5 nm for the cemented sandstone (Fig. 6b), closely resembles that of a well cemented tight shale (e.g. Katsube and Williamson, 1994, 1998). The pore-size distribution pattern dominated by ϕ_{ip} (d=25 nm to 10 µm) with a major mode (d_2) value of 300–800 nm representing the mudstones of this suite (Fig. 6c) is typical of an undercompacted, poorly sorted or coarse-grained mudstone (Katsube et al., 1995; Katsube
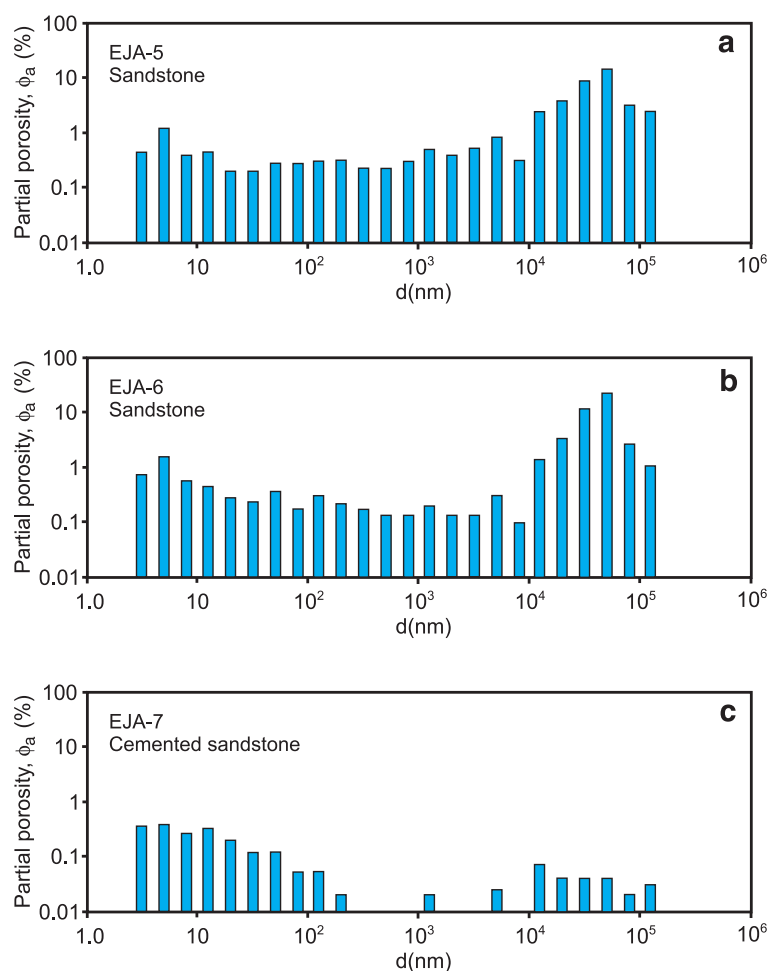

Figure 3.

*Pore-size distributions for two unconsolidated sandstones **a)** sample EJA-5 (906.2 m) and **b)** sample EJA-6 (919.1 m); and a tight cemented sandstone **c)** sample EJA-7 (925.9 m). The 'd' represents the pore sizes. A logarithmic scale is used for the vertical axis.*

and Williamson, 1998). It should be noted, however, that these mudstone samples also display a minor pore-size body of ϕ_{np} (d=2.5–25 nm) with a minor mode (d_1) value of 5 nm.

A reasonably good correlation exists between the three porosities: ϕ_{np}, ϕ_{ip}, and ϕ_{mp}, and the clay, silt, and sand contents, respectively as shown in Figure 7. This suggests that the three porosities represent some type of quantitative information on their corresponding grain types. The depth relationships for ϕ_{np}, $\phi_{ip}+\phi_{mp}$, and ϕ_E are displayed in Figure 8. These results indicate that ϕ_E shows a relatively small change (ϕ_E =23–36%) with depth or rock type, except for the tight sandstone (ϕ_E =2.2%), regardless of the considerable difference between sandstone and mudstone textures. The $\phi_{ip}+\phi_m$ varies little with depth (Fig. 8) for both mudstone units (MS-1 and MS-2), but shows an increase for the sandstone (910–930 m), likely reflecting a considerable increase in sand content, as would be expected. The ϕ_{np} values tend to show an increase with depth towards the top of both upper and lower sandstone formations at 896.8 m and 950 m depths, likely reflecting a clay content increases with depths for both mudstone units. As a result of these analyses, a framework-supported texture model has been developed for these
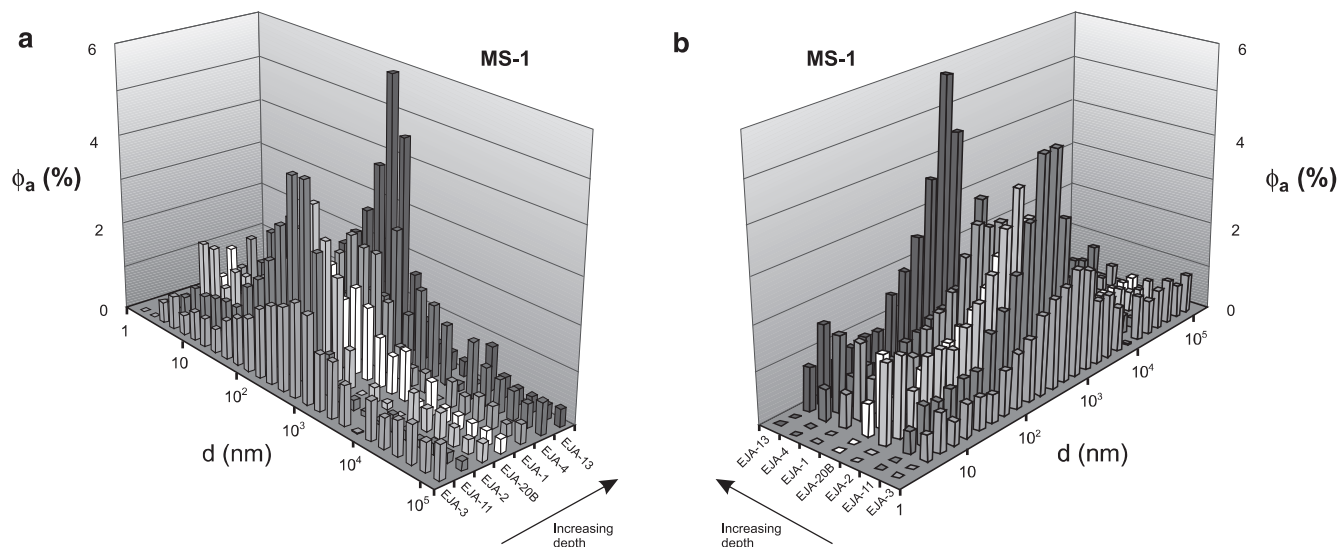

Figure 4. a), b) Two 3-D views of a set of pore-size distributions for seven mudstone samples from the mudstone unit MS-1 (890–920 m). The parameters ϕ_a and 'd' represent the partial porosity and pore sizes, respectively.
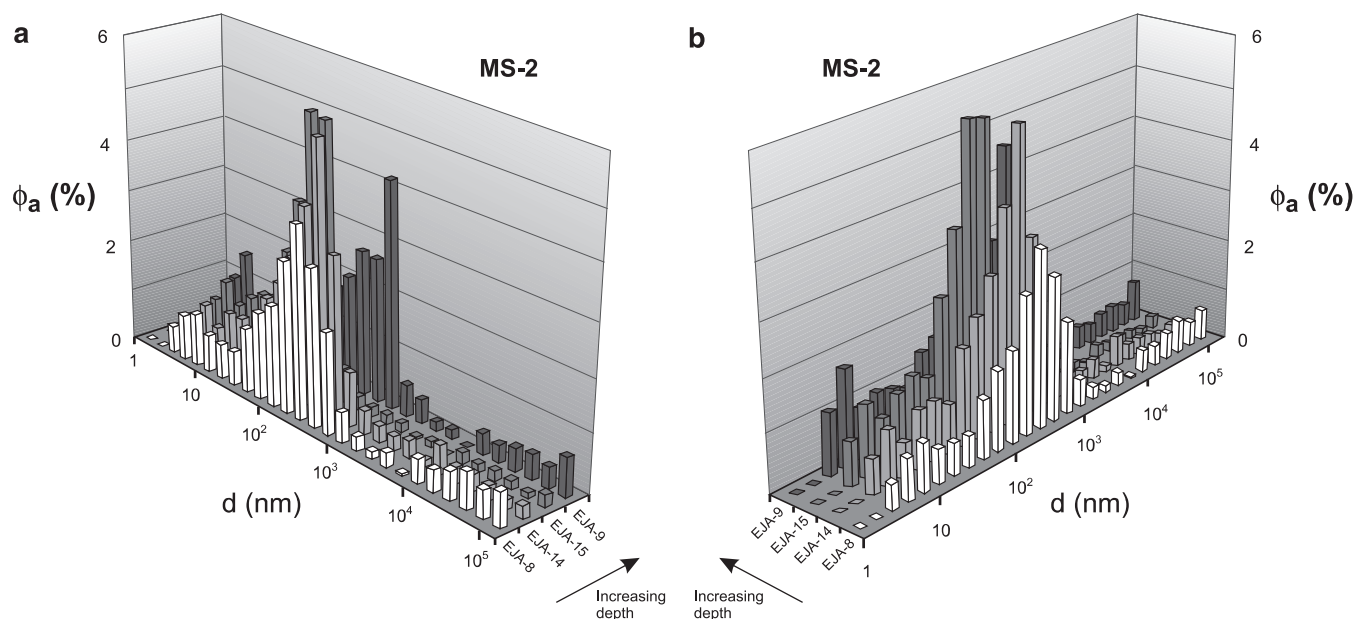

Figure 5. a), b) Two 3-D views of a set of pore-size distributions for four mudstone samples from the mudstone unit MS-2 (926–955 m). The parameters ϕ_a and 'd' represents the partial porosity and pore sizes, respectively.

samples. It consists of a framework of silt and sand grains with matrix material (clay) filling the intergranular pore spaces (Fig. 9), from degrees of about zero for the sandstone samples to about 100% for a well compacted mudstone.

The results of these studies have indicated that, regardless of their shallow burial depths (880–950 m), these mudstone samples have a relatively well developed framework-supported texture. This is likely due to their high silt and sand content (75–100%) in addition to a past history of a burial depth greater than the present. Although silt and sand generally dominate the texture, it has been indicated that the minor matrix content may be sufficient to dominate the petrophysical characteristics (permeability, storage pore sizes) for most of the mudstone samples. At present, there is no commonly known petrophysical parameter available to indicate whether the

framework or matrix dominates the fluid transport characteristics, other than actual permeability or formation factor measurements. If the matrix dominates, then the mudstone is expected have low permeabilities (k_L) and the minor mode (d_1, Fig. 6) values should be used for their estimation (Katsube et al., 1997). On the other hand, if the framework dominates, then the permeabilities are expected to be very large, and it would be reasonable to use a method commonly used to calculate sandstone permeabilities (e.g. Uchida, 1987). In the latter case, median pore-size (d_{MD}, Table 3), pore surface area (A), and ϕ_{Hg} are used to derive the high permeability (k_H) values. Data obtained from other publications (Uchida et al., 1999; T.J. Katsube, T. Uchida, S.R Dallimore, K.A., Jenner, T.S. Collett, and S. Connell, unpub. manuscript, 1999) are listed in Table 3 to calculate these parameters, in addition to
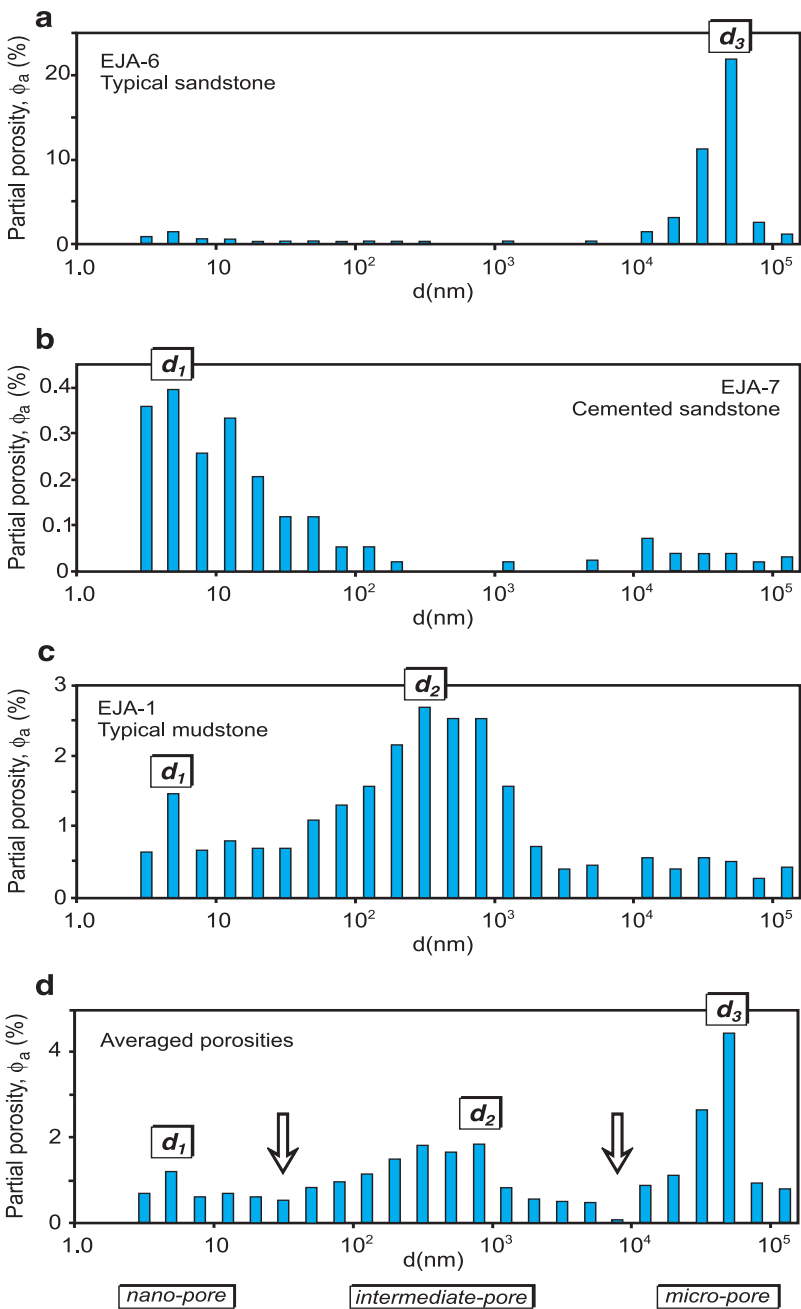

Figure 6.

Typical pore-size distributions for the a) sandstone, b) tight sandstone, and c) mudstone samples used in this study, and their d) average pore-size distribution (tri-modal distribution). The d_1, d_2, and d_3 are the modes for each of the three pore-size distribution bodies.
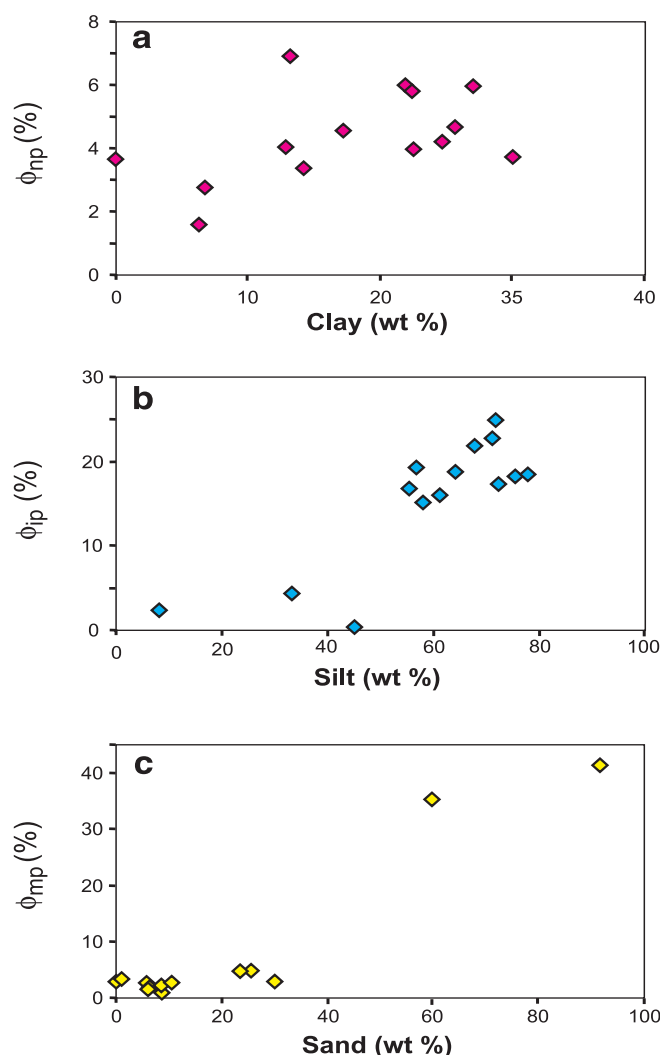
Figure 7. *Relationships between porosities and grain-size contents **a)** for nano-pore porosity (ϕ_{np}) and clay, **b)** intermediatepore porosity (ϕ_{ip}) and silt, and **c)** micro-pore porosity (ϕ_{m}) and sand.*

the two types of calculated permeability values. The k_H values for the sandstone, cemented sandstone, and mudstone are 6×10^{-16} m^2 to 2.6×10^{-15} m^2, 4.3×10^{-16} m^2, and 1×10^{-19} m^2 to 2×10^{-16} m^2, respectively (Table 3). The k_L values for the cemented sandstone and mudstone are 1×10^{-21} m^2 and 1×10^{-21} m^2 to 1.4×10^{-21} m^2, respectively (Tables 3), a considerable difference between the two sets of calculated permeabilities. The k_H values for the sandstone (6×10^{-16} m^2 to 2.6×10^{-15} m^2) and the k_L values for the cemented sandstone (1×10^{-21} m^2) are reasonable (Katsube and Connell, 1998), because the former appears to be relatively clean sandstone and the latter a very tight sandstone with a very low effective porosity (ϕ_E=2.2%). The k_H (1×10^{-19} m^2 to 2×10^{-16} m^2) for the mudstone may be questionable, however, because of the relatively high matrix content.

There are currently no known standard petrophysical parameters that can provide quantitative information on the storage pore sizes, although mode d_2 and ϕ_S may provide some information on their possible range. Quantitative analysis of the SEM images may provide more accurate information on the storage pore-size distribution. However, since the storage pore sizes could be related to their surface area or the matrix content within the intergranular pore spaces, the k_H values may provide relevant information. Equation 7 (Table 3) for the calculated permeability k_H contains a term, $\phi_{Hg}(d_{MD}/2)^2/A$, which is directly or indirectly related to most of these parameters. The k_H as a function of depth (h) is shown in Figure 1.

MUDSTONE AND SANDSTONE TEXTURE

Mineralogical and textural analyses were performed on selected sandstone and mudstone samples collected from the Mallik 2L-38 well site using visual, thin section, back-scatter of the scanning electron microscope (SEM), and X-ray diffraction analyses (XRD). Detailed visual examination of selected mudstone samples immediately above the two gas-hydrate-bearing formations indicate that samples EJA-1, EJA-2, and EJA-15 have visibly layered to semilayered texture, with sample EJA-1 displaying one or two very thin (<1 mm) silt layers that are solidly cemented (Fig. 10). Sample EJA-9 is bioturbated (Jenner et al., 1999) and lacks any visible layering. The mudstone texture was analyzed by microscopic examination of thin sections from resin-saturated rock specimens and SEM secondary imaging of carbon-coated rock-specimen surfaces. Results of the XRD analysis are listed in Table 4. The total clay content (T-Cl) for the mudstone samples is 25–27%.

Examples of thin section and SEM analyses are displayed in Figures 11 and 12 for a typical mudstone and the cemented sandstone. Figure 11a shows a framework-supported texture and Figures 11b and 11c show that the intergranular pore spaces are generally filled with a clay matrix (sample EJA-1). The blue sections represent interconnected pore spaces. Figure 12a shows well cemented texture, the cement being dominantly dolomite, and Figure 12b shows that the primary intergranular pores are very widely spaced and isolated by dolomite-cemented sand (sample EJA-7). These results support the mudstone framework-supported texture model (Fig. 9) with the intergranular pore spaces filled with fine-grained (clay) material, a model proposed as a result of the pore-size distribution studies. On the basis of previous work (Katsube and Williamson, 1998), the fact that the minor mode (d_1) values are in the range of 5–7.9 nm (Fig. 3c), suggests that the clay material is highly compacted. The pore-size distribution and this SEM data suggest pore diameters of 5–7.9 nm and 100–2000 nm, respectively, for the connecting and storage pores of the clay matrix, and 5–50 µm for the intergranular storage pore space without the clay matrix, as shown in Figure 9.

PERMEABILITY CHARACTERISTICS

Low permeability (k) measurements have been carried out on four mudstone samples, two (sample EJA-1: 896.8 m, and sample EJA-2: 896.4 m) from immediately above the upper gas-hydrate-bearing zone, and two (sample EJA-9: 949.4 m, and sample EJA-15: 944.5 m) from above the lower gas-hydrate-bearing zone. The results are shown in Figure 13, displaying unexpectedly low permeabilities ($2x10^{-21}$ m^2 to $2x10^{-19}$ m^2) for mudstone samples from these shallow depths. The initial k-decrease to effective pressures (P_E) of about 10 MPa, close to the current in situ hydrostatic pressure, is due to closing of the destressed pores, a result of samples being extracted from in situ conditions. The k-curves for P_E>10 MPa represent the true mudstone permeability characteristics.

These samples were selected to determine if the mudstone formations immediately above the upper and lower gas-hydrate-bearing formations contained a seal. These measured results of low permeability indicate that the calculated results (Table 2) for low permeabilities (k_L=$1x10^{-21}$ m^2 to $1.4x10^{-21}$ m^2) are generally more realistic than those for the high permeabilities (k_H=$1x10^{-19}$ m^2 to $2x10^{-16}$ m^2). This implies that

the minor matrix content has a controlling effect on the fluid transport characteristics of, at least, these four mudstone samples (samples EJA-1, EJA-2, EJA-9, EJA-15). While such low measured permeabilities ($2x10^{-21}$ m^2 to $2x10^{-19}$ m^2) have been reported for P_E values equivalent to the depths of these samples (Katsube and Connell, 1998), it is surprising that the minor matrix content would dominate the transport characteristics of mudstone with such a high silt/sand content at these shallow depths. These results also suggest that the maximum burial depths for these mudstone samples are likely to have been greater than their current depths. These low measured permeability values imply good to relatively good seal qualities.

PRESSURE CHARACTERISTICS OF PORE STRUCTURE

The pressure characteristics of effective porosity (ϕ_{EW}) and apparent formation factor (F_a) have been determined for two mudstone samples (samples EJA-1 and EJA-2; J.M. Loman, T.J. Katsube, N. Perez, and S.R. Dallimore, unpub. manuscript, 1999). These samples are identical to those used for two of the low-permeability (k) measurements, but separate
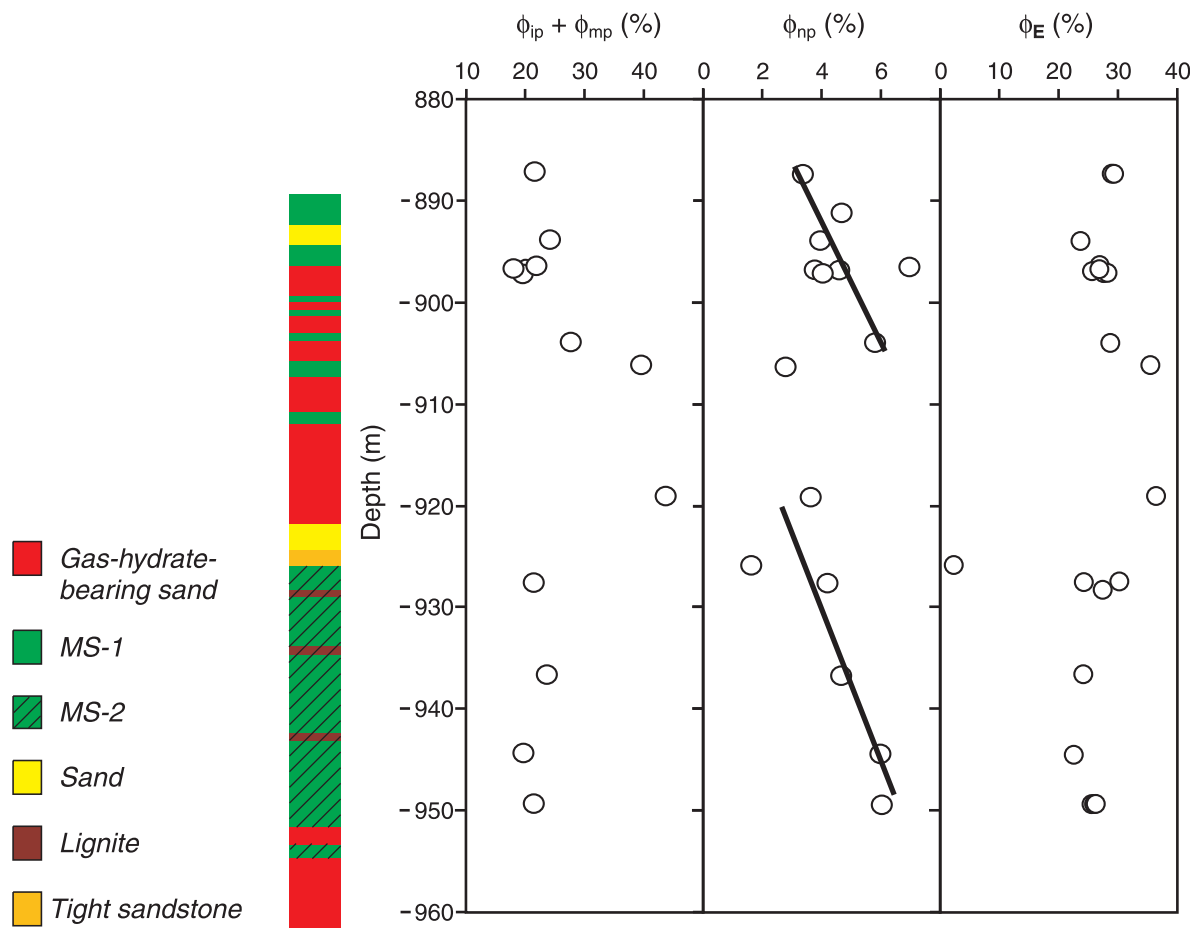

Figure 8. *Porosity-depth relationship for effective porosity (ϕ_E), represented by helium porosity (ϕ_{he}), nano-pore porosity (ϕ_{np}), and the sum of intermediate and micro-pore porosities (ϕ_{ip}+ϕ_{mp}). The very low ϕ_E and ϕ_{np} values at 926–927 m are due to the cemented sandstone.*

specimens were used for these measurements. The ϕ_{EW} values, in this case, represent the effective porosity of a water-saturated mudstone, and its pressure characteristics are determined by monitoring the water expelled from the sample under increasing confining pressure. Details for this technique have previously been reported (Loman et al., 1993). The results for this study are shown in Figure 14. The ϕ_{EW} for these results are larger than the effective porosities (ϕ_E) determined by the helium porosimetry method for reasons explained below. The pressure characteristics for true formation factor (F) was determined, first by measuring F_a at different confining pressures, and then by applying the conversion technique of Katsube (1999) to determine the true formation

factor. Subsequently, by use of a combination of new and previously reported techniques (e.g. Walsh and Brace, 1984; Katsube and Walsh, 1987; Katsube, et al., 1991), the pressure characteristics of storage porosity (ϕ_s) and connecting porosity (ϕ_c) have been determined. These results are shown in Figure 14.

The results in Figure 14 show ϕ_{EW} and ϕ_c decreasing with increased confining pressure (P_c), as would be expected, but with ϕ_s showing little to no change with pressure. The little
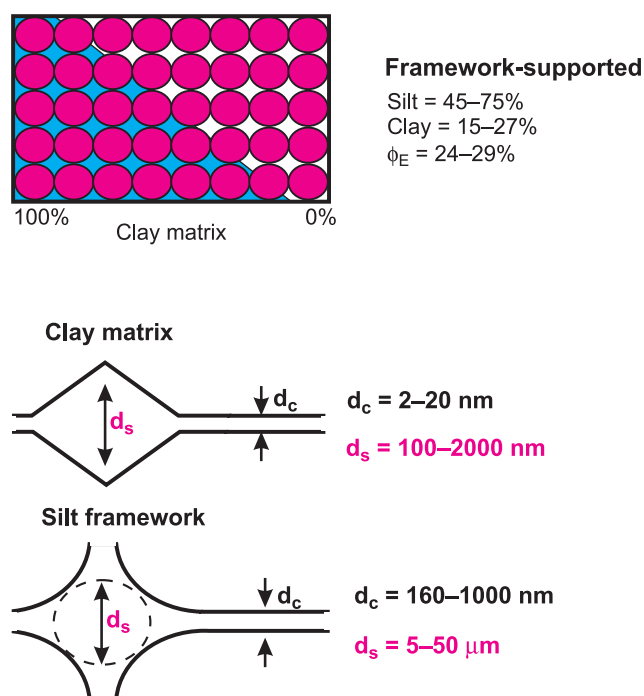
MUDSTONE TEXTURE

Framework-supported
Silt = 45–75%
Clay = 15–27%
ϕ_E = 24–29%

100%
Clay matrix
0%

Clay matrix

d_c = 2–20 nm

d_s = 100–2000 nm

Silt framework

d_c = 160–1000 nm

d_s = 5–50 μm

Figure 9. *Model of a framework-supported texture with a varying degree of clay matrix filling the intergranular pore spaces.*

(a) High - k

EJA-9

(b) Intermediate - k

EJA-2   EJA-15

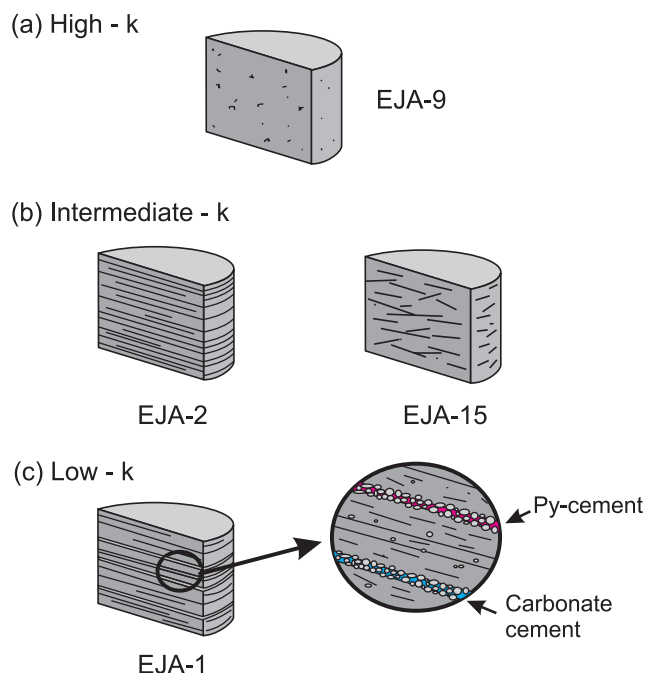(c) Low - k

Py-cement

Carbonate cement

EJA-1

Figure 10. *Block diagrams of mudstone samples displaying visually physical features of importance in relation to their permeability (k) characteristics: **a)** relatively high k values (sample EJA-9, h=949.4 m, k=1x10^{-19} m^2 to 2x10^{-19} m^2), **b)** intermediate k values (samples EJA-2 and EJA-15, h=949.4 m and 944.5 m, k=5x10^{-21} m^2 to 2x10^{-20} m^2), and **c)** extremely low k values (sample EJA-1, h=896.8 m, k=1x10^{-21} m^2 to 2x10^{-19} m^2). The symbol 'h' represents the sample depth, and Py represents pyrite.*

Table 4. Bulk and clay mineralogy (%) data determined by X-ray diffraction (XRD) for seven mudstone samples collected from the Mallik 2L-38 well site.

Samples	Qtz (%)	Pl (%)	KF (%)	Cal (%)	Dol (%)	Py (%)	T-Cl (%)	Kln (%)	Chl (%)	Ill (%)	Smc (%)	MX (%)	%MX (%)
EJA-1	65	4	0	2	0	2	27	5	4	15	3	3	15
EJA-2	70	3	2	0	0	0	25	5	3	14	2	2	15
EJA-7	66	2	0	0	26	0	6	1	1	3	2	1	51
EJA-8	49	7	1	0	0	2	41	6	4	28	3	0	–
EJA-9	60	4	1	0	0	Tr	35	5	3	25	–	0	–
EJA-15	55	1	1	0	0	0	43	9	6	26	–	0	–
EJA-20	50	1	Tr	0	0	2	47	7	6	31	–	0	–

Qtz = Quartz	Py = Pyrite	Ill = Illite
Pl = Plagioclase	T-Cl = Total clay	Smc = Smectite
KF = K-feldspar	Kln = Kaolinite	MXL = Mixed layer (MXL)-illite/smectite
Cal = Calcite	Chl = Chlorite	%MX = Percentage of illite in MXL
Dol = Dolomite	Tr = Trace	– = No data

change in ϕ_s is probably due to the fact that these mudstone samples already have a well developed framework-supported texture, as previously suggested, and that the framework grains of silt and sand which are in contact with each other are resisting any mechanical change in intergranular pore space. The fact that ϕ_c shows considerable decrease with increased

confining pressure indicates that the connecting pores have little protection against collapse under increased pressure. This is likely due to the connecting pore shapes being sheet-like, and the pore walls being held apart by free and loosely bound water molecules. The first five water molecular layers on each pore wall are considered to be strongly bound, and
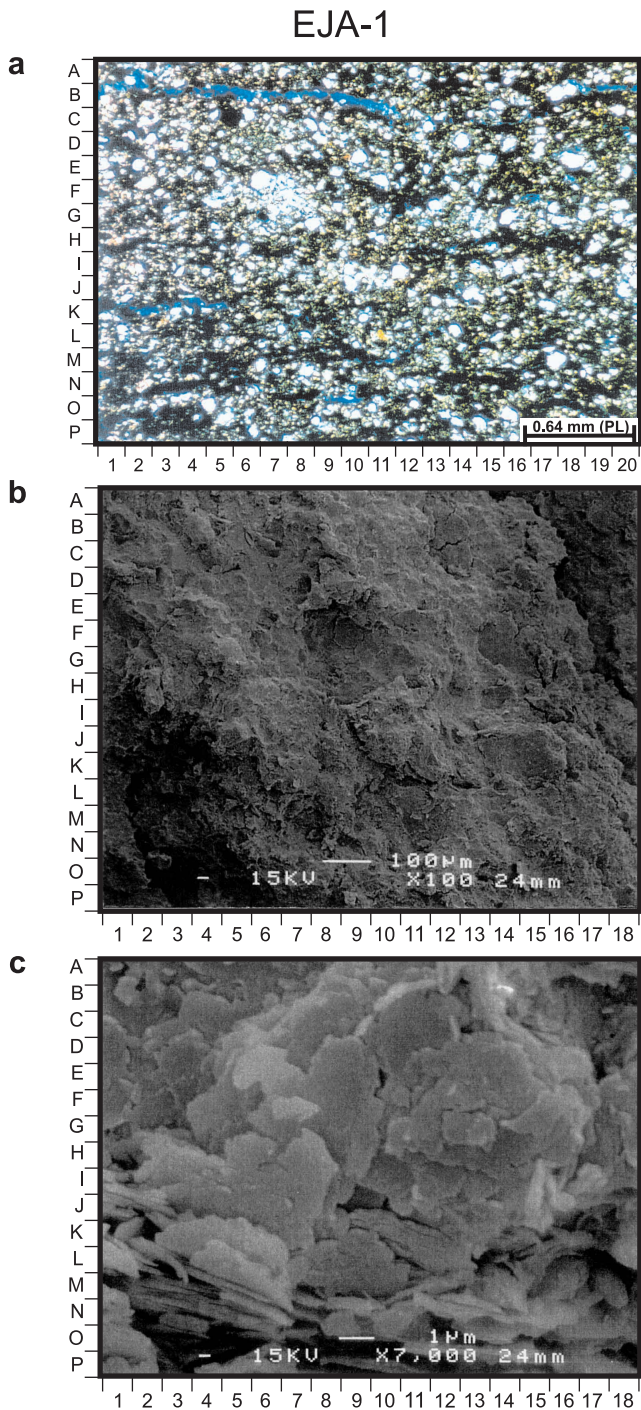

Figure 11. *Thin section image **a)**, and SEM images **b)** and **c)** for a mudstone (sample EJA-1, 896.8 m). The blue sections in **a)** indicate interconnected pore spaces.*
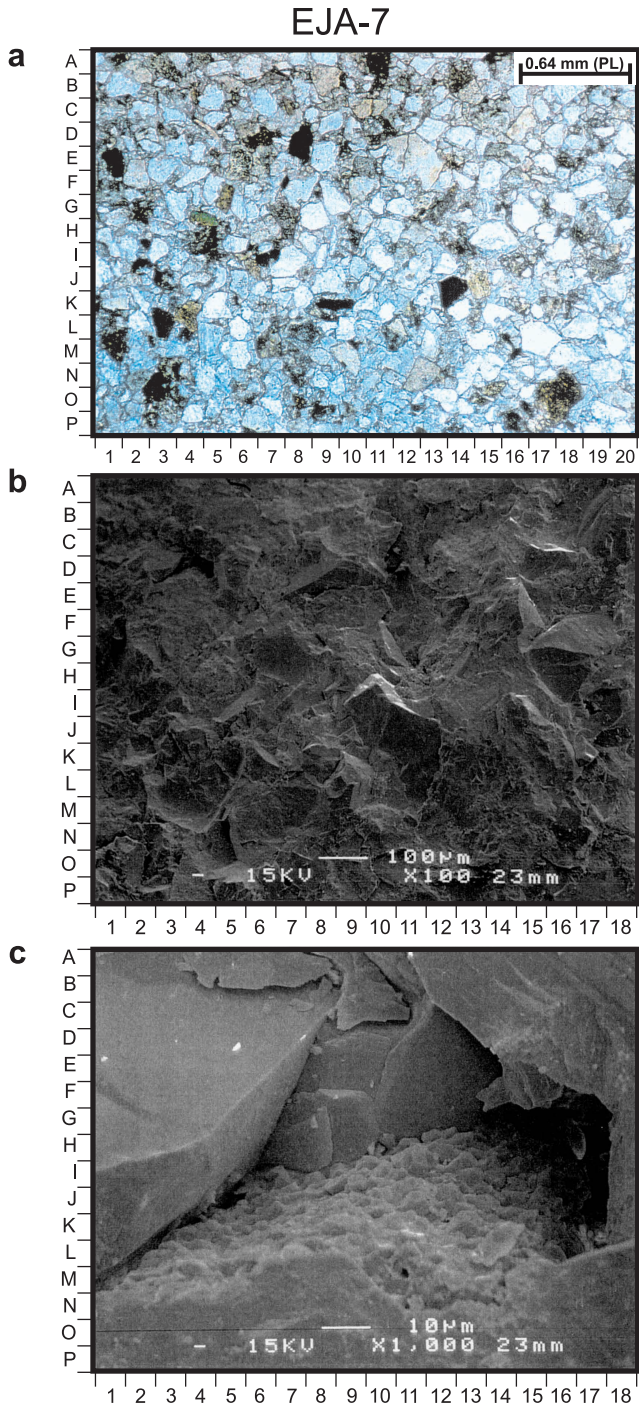

Figure 12. *Thin section image **a)**, and SEM images **b)** and **c)** for a tightly cemented sandstone sample (EJA-7, 925.9 m). The blue sections in **a)** indicate interconnected pore spaces.*

resist considerably high mechanical pressure (Hinch, 1980). It is likely that only the loosely bound water and free water are expelled under increased confining pressure. Much of the free water and loosely bound water in these connecting pores are probably absent in the dry mudstone samples being used for helium porosimetry.

DISCUSSION

Pore-structure model

The fact that the main pore-size distribution group is the intermediate porosity (ϕ_{ip}) with a mode (d_2) of 520–790 nm, suggests (Katsube and Williamson, 1998) that these mudstone samples are coarse grained, undercompacted, and poorly sorted. The suggestion that they are coarse grained is supported by the grain-size data showing a high silt content (56–78%) or a combined silt and sand content (77–87%, Table 3), and by the thin section images displaying an abundance of coarse grains (e.g. Fig. 11a). The undercompaction is supported by the relatively high effective porosity values of 24–30% (Table 1) and by the scanning electron microscope (SEM) images (e.g. Fig. 11b, c) showing a lack of well compacted texture. The poorly sorted texture is obvious from the
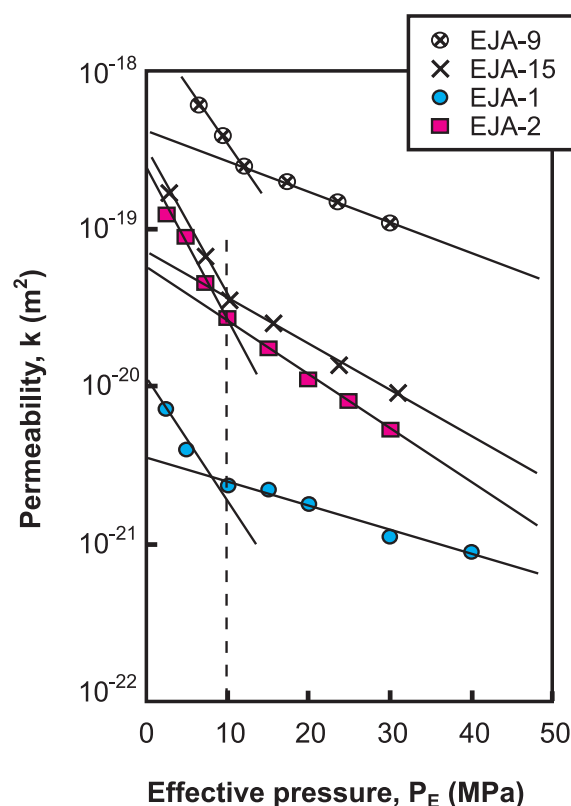

Figure 14. Effective porosity (ϕ_{EW}), storage porosity (ϕ_s), and connecting porosity (ϕ_c) as a function of effective pressure (P_E) for two mudstone samples, EJA-1 and EJA-2. This parameter, ϕ_{EW}, represents the effective porosity of a water-saturated sample.

thin section image (Fig. 11a). The mudstone nano-porosity (ϕ_{np}) is a minor pore-size distribution group (Fig. 6c), suggesting the existence of fine-grained material (clay) that might be of significance. This is supported by the grain-size analysis data showing a clay content of 13–25% (Table 2), and the X-ray diffraction (XRD) data showing a clay content of 25–27% (Table 4). The fact that the minor mode (d_1) values are in the range of 5–7.9 nm (Table 2), suggests that the clay material is highly compacted (Katsube and Williamson, 1998). As a results of these analyses, a framework-supported texture model (Fig. 9) is proposed for the mudstone samples used in this study. This model suggests the intergranular pore spaces are filled with loose to tightly compacted fine-grained (clay) material. The pore-size distribution and SEM data suggest pore diameters of 5–7.9 nm and 100–2000 nm, for the connecting and storage pores of the clay matrix, respectively, and 5–50 μm for the silt and sand intergranular storage pore space without the clay matrix.

Two mudstone units

The relationships between nano-pore porosity (ϕ_{np}) and clay, intermediate-pore porosity (ϕ_{ip}) and silt, and micro-pore porosity (ϕ_{mp}) and sand contents (displayed in Fig. 7a–7c) have suggested that all three porosity types represent some type of quantitative information on their corresponding grain types. The sample depth relationships for the three porosities

Figure 13. Permeability (k) as a function of effective pressure (P_E) for four mudstone samples: EJA-1 (h=896.8 m), EJA-2 (h=896.4 m), EJA-9 (h=949.4 m), and EJA-15 (h=944.5 m). The symbol "h" represents depth in the borehole.
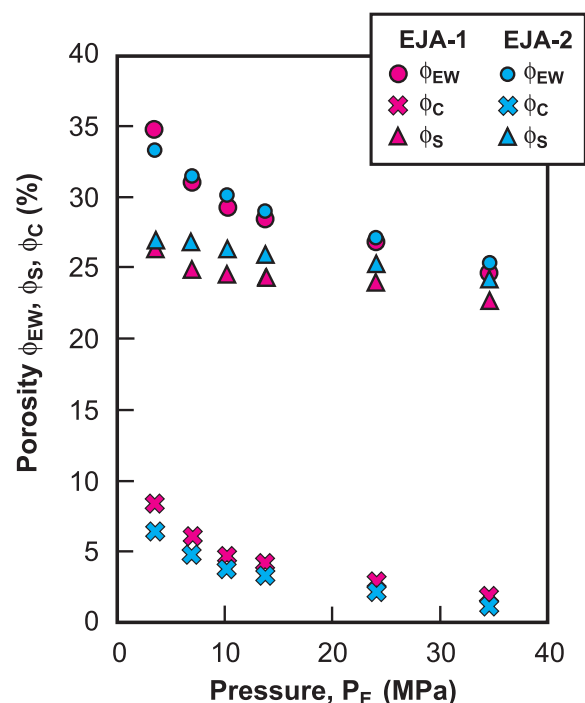
(ϕ_{np} and $\phi_{ip}+\phi_{mp}$) and that of ϕ_{EW} displayed in Figure 8 indicate that effective porosities (ϕ_E) show little change (ϕ_E =24–30%) with depth or rock type, regardless of the considerable difference in sandstone and mudstone textures, except for the tight sandstone (925–926 m). The $\phi_{ip}+\phi_{mp}$ values vary little with depth (Fig. 8c), but show an increase for the depths of 910–930 m, likely reflecting the considerable increase in sand content for the sandstone, as would be expected. The tendency for ϕ_{np} to show a slight increase with depth (Fig. 8b) likely reflects a increase in clay content with depth. This confirms the framework-supported texture model with the varying degree of clay matrix filling the intergranular pore spaces (Fig. 9). The break in the ϕ_{np} increase between 905 m and 920 m reflects a boundary between the two mudstone units, MS-1 and MS-2. These two mudstone units show a slight difference in their pore-size distribution, with unit MS-2 lacking pores in the 1–16 µm pore-size range, probably reflecting the absence of coarser grained silt.

Permeability control

The mudstone pore-size distribution data suggested the existence of a minor content of fine-grained material (clay) that might be of significance. The fact that the measured permeabilities contain very low values ($2x10^{-21}$ m^2 to $2x10^{-19}$ m^2) implies that this suggestion is confirmed and that the minor matrix content has a controlling effect on the fluid transport characteristics of the mudstone immediately above the gas-hydrate-bearing formations. While such low measured permeabilities ($2x10^{-21}$ m^2 to $2x10^{-19}$ m^2) have been reported for depths similar to those of these samples (Katsube and Connell, 1998), it is surprising that the minor matrix content would dominate the transport characteristics of mudstone with such a high silt/sand content at these shallow depths. These results also support the suggestion that the maximum burial depths of the mudstone are likely greater than their current depths. These low measured permeability values imply good to relatively good seal qualities.

Storage pore-size distribution

While there is considerable information on the connecting pore sizes available from the pore-size distribution analysis, information on the storage pore-sizes is very limited. Thin section, SEM, and other indirect information (pore-size distribution) have suggested 100–2000 nm for storage pore sizes in the matrix and 5–50 µm for the intergranular storage pore space barren of clay matrix (Fig. 9). This applies to both sandstone and mudstone. Since the storage pore sizes, in principle, could be related to porosity and matrix content (surface area) in the intergranular pore spaces, the calculated high permeabilities (k_H) may provide some relevant qualitative information, because they are influenced by a term (Table 3) which is directly or indirectly related to these parameters (Uchida, 1987). The k_H as function of depth is shown in Figure 1, displaying a good correlation with the gas hydrate content. The only quantitative information available on the storage pores is storage porosity (ϕ_S), which is 12–17% for mudstone.

Hydrocarbon seal types

The four mudstone samples with permeability (k) measurements can be divided into three groups (Fig. 13) on the basis of their k values: the one displaying relatively high k values (sample EJA-9, h=949.4 m, k=$1x10^{-19}$ m^2 to $2x10^{-19}$ m^2), the two displaying intermediate k values (EJA-2 and EJA-15, h=949.4 m and 944.5 m, k=$5x10^{-21}$ m^2 to $2x10^{-20}$ m^2 respectively) and the one displaying extremely low k values (EJA-1, h=896.8 m, k=$1x10^{-21}$ m^2 to $2x10^{-21}$ m^2). The symbol 'h' represents the depth. No obvious relationship is seen between their ϕ_E (23–27%) and clay content (13–22 weight per cent). Samples EJA-1, EJA-2, and EJA-15 have visibly layered to semilayered texture, with sample EJA-1 displaying one or two very thin (<1 mm) silt layers that are solidly cemented (Fig. 10). This may be the reason for it displaying the lowest k values. Sample EJA-9 is bioturbated and lacks any visible layering, which may be the reason for its higher k values.

Implication for gas hydrate accumulation

The pore-structure characteristics likely controlling growth and distribution of gas hydrate are the formation permeability and the storage pore sizes. This study shows that a very low permeability (k=$1x10^{-21}$ m^2 to $2x10^{-20}$ m^2) but thin mudstone layer overlies the upper gas hydrate formation, and a somewhat low permeability (k=$1x10^{-20}$ m^2 to $2x10^{-19}$ m^2) but thicker mudstone layer overlies the lower gas hydrate formation. These permeabilities imply that these mudstone layers could form barriers to the flow of hydrocarbons. While the storage pore sizes are likely to vary from 100–2000 nm to 5–50 µm, with the sandstone expected to be consistently at the higher end, the mudstone storage pore sizes show evidence of varying considerably. No parameter to quantitatively monitor this variation with depth has been suggested to date. However, there are indications that the calculated high permeability (k_H) could play a qualitative role of such, although their absolute values do not necessarily represent the true measured values for the mudstone. They do however, likely represent the true values of the sandstone.

CONCLUSIONS

The results of this study indicate that, regardless of their shallow burial depths (880–950 m), these samples have a relatively well developed framework-supported texture. This is likely due to their high silt and sand content (75–100%), in addition to a past history of an overburden pressure higher than that of the present. The texture model developed for these samples is a framework of silt and sand grains with matrix material (clay) filling the intergranular pore spaces, from degrees close to zero (sandstone) to 100% (relatively well compacted mudstone). Although silt and sand generally dominate the texture, there are indications that the minor matrix content dominates the petrophysical characteristics (permeability, storage pore sizes) of these mudstone samples. This minor matrix content dominance is confirmed by the measured mudstone permeabilities which contain very low values, implying that their connecting pores are represented

by those of the matrix material, which have an average diameter of about 5 nm. It is suggested that this minor matrix content also controls the storage pore sizes. These facts indicate that the matrix material, existing mainly in the mudstone formations, is likely to have a controlling effect on the distribution of the gas hydrate in these sedimentary sequences, by controlling both the flow of fluids (including gas) and the necessary storage pore sizes that allow their growth. The fine layered mudstone texture may also play a significant role in controlling the flow of fluids, as suggested by the mudstone sample with the thin (<1 mm), cemented, coarser grained layers displaying the lowest permeability.

ACKNOWLEDGMENTS

The authors express their thanks to M.A. Williamson (GSC Atlantic) for critically reviewing this paper, and to J. Bloch (Scealu Modus, New Mexico, U.S.A.) for his comments on the geological section of this paper.

REFERENCES

Agterberg, F.P., Katsube, T.J., and Lew, S.N.
1984:   Statistical analysis of granite pore size distribution data, Lac du Bonnet batholith, eastern Manitoba; *in* Current Research, Part A; Geological Survey of Canada, Paper 84-1A, p. 29–37.

Collett, T.S., Lewis, R., Dallimore, S.R., Lee, M.W., Mroz, T.H., and Uchica, T.
1999:   Detailed evaluation of gas hydrate reservoir properties using JAPEX/JNOC/GSC Mallik 2L-38 gas hydrate research well downhole well-log displays; *in* Scientific Results from JAPEX/JNOC/GSC Mallik 2L-38 Gas Hydrate Research Well, Mackenzie Delta, Northwest Territories, Canada, (ed.) S.R. Dallimore, T. Uchida, and T.S. Collett; Geological Survey of Canada, Bulletin 544.

Dixon, J., Dietrich, J.R., and McNeil, D.H.
1992:   Upper Cretaceous to Pleistocene sequence stratigraphy of the Beaufort-Mackenzie and Banks Island areas, northwest Canada; Geological Survey of Canada, Bulletin 407, 90 p.

Hinch, H.H.
1980:   The Nature of Shales and the Dynamics of Hydrocarbon Expulsion in the Gulf Coast Tertiary Section; AAPG Publication, Tulsa, Oklahoma, p. 1–18.

Jenner, K.A., Dallimore, S.R., Clark, I.D., Paré, D., and Medioli, B.E.
1999:   Sedimentology of gas hydrate host strata from the JAPEX/JNOC/GSC Mallik 2L-28 gas hydrate research well; *in* Scientific Results from JAPEX/JNOC/GSC Mallik 2L-38 Gas Hydrate Research Well, Mackenzie Delta, Northwest Territories, Canada, (ed.) S.R. Dallimore, T. Uchida, and T.S. Collett; Geological Survey of Canada, Bulletin 544.

Katsube, T.J.
1992:   Statistical analysis of pore-size distribution data of tight shales from the Scotian Shelf; *in* Current Research, Part E; Geological Survey of Canada, Paper 92-1E, p. 365–372.
1999:   True formation factor determination by nonlinear curve fitting; *in* Current Research 1999-D; Geological Survey of Canada, p. 27–34.

Katsube, T.J. and Collett, L.S.
1975:   Electromagnetic propagation characteristics of rocks; *in* The Physics and Chemistry of Rocks and Minerals, (ed.) R.G.J. Strens; John Wiley & Sons Ltd., London, U.K., p. 279–295.

Katsube, T.J. and Connell, S.
1998:   Shale permeability characteristics; *in* Current Research, 1998-E, Geological Survey of Canada, p. 183–192.

Katsube, T.J. and Issler, D.R.
1993:   Pore-size distribution of shales from the Beaufort-MacKenzie Basin, northern Canada; *in* Current Research, Part E; Geological Survey of Canada, Paper 93-1E, p. 123–132.

Katsube, T.J. and Walsh, J.B.
1987:   Effective aperture for fluid flow in microcracks; International Journal of Rock Mechanics and Mining Sciences and Geomechanics, Abstracts, v. 24, p. 175–183.

Katsube, T.J. and Williamson, M.A.
1994:   Effects of diagenesis on shale nano-pore structure and implications for sealing capacity; Clay Minerals, v. 29, p. 451–461.
1998:   Shale petrophysical characteristics: permeability history of subsiding shales; *in* Shales and Mudstones II, (ed.) J. Schiber, W. Zimmerle, and P.S. Sethi; Stattgard, Germany, p. 69–91.

Katsube, T.J., Best, M.E., and Mudford, B.S.
1991:   Petrophysical characteristics of shales from the Scotian shelf; Geophysics, v. 56, p. 1681–1689.

Katsube, T.J., Bloch, J., and Cox, W.C.
1998:   The effect of diagenetic alteration on shale pore-structure and its implications for abnormal pressures and geophysical signatures; *in* Overpressures in Petroleum Exploration Workshop, Proceedings Volume, April 7–8, 1998, Pau, France; Elf Exploration Production, France, p. 1/9–9/9.

Katsube, T.J., Bloch, J., and Issler, D.R.
1995:   Shale pore structure evolution under variable sedimentation rates in the Beaufort-MacKenzie Basin; *in* Proceedings of the Oil and Gas Forum' 95, Energy from Sediments; Geological Survey of Canada, Open File 3058, p. 211–215.

Katsube, T.J., Dorsch, J., and Connell, S.
1997:   Pore surface area characteristics of the Nolichucky Shale within the Oak Ridge Reservation (Tennessee, U.S.A.): implication for fluid expulsion efficiency; *in* Current Research, 1997-E, Geological Survey of Canada, p. 117–124.

Katsube, T.J., Williamson, M., and Best, M.E.
1992:   Shale pore structure evolution and its effect on permeability; *in* Symposium Volume III of the Thirty-Third Annual Symposium of the Society of Professional Well Log Analysts (SPWLA); The Society of Core Analysts Preprints, Oklahoma City, Oklahoma, June 15–17, 1992, Paper SCA-9214, p. 1–22.

Loman, J.M., Katsube, T.J., Correia, J.M., and Williamson, M.A.
1993:   Effect of compaction on porosity and formation factor for tight shales from the Scotian Shelf, offshore Nova Scotia; *in* Current Research, Part E; Geological Survey of Canada, Paper 93-1E, p. 331–335.

Miyairi, A., Akihisa, K., Uchida, T., Collett, T.S., and Dallimore, S.R.
1999:   Well-log interpretation of gas-hydrate-bearing formations in the Mallik2L-38 gas hydrate research well; *in* Scientific Results from JAPEX/JNOC/GSC Mallik 2L-38 Gas Hydrate Research Well, Mackenzie Delta, Northwest Territories, Canada, (ed.) S.R. Dallimore, T. Uchida, and T.S. Collett; Geological Survey of Canada, Bulletin 544.

Ohara, T., Dallimore, S.R., and Fercho, E.
1999:   Drilling operations, JAPEX/JNOC/GSC Mallik 2L-38 gas hydrate research well; *in* Scientific Results from JAPEX/JNOC/GSC Mallik 2L-38 Gas Hydrate Research Well, Mackenzie Delta, Northwest Territories, Canada, (ed.) S.R. Dallimore, T. Uchida, and T.S. Collett; Geological Survey of Canada, Bulletin 544.

Rootare, H.M.
1970:   A review of mercury porosimetry; Perspectives of Powder Metallurgy, v. 5, p. 225–252.

Uchida, T.
1987:   Pore-size distribution and the evaluation of permeability in reservoir rocks - a proposal of empirical expressions with regard to petrological properties of pores; Journal of The Japanese Association for Petroleum Technology, v. 52, no. 1, p. 1–11.

Uchida, T., Matsumoto, R., Waseda, A., Okui, T., Yamada, K., Uchida, T. Okada, S., and Takana, O.
1999:   Summary of physicochemical properties of natural gas hydrate and associated gas-hydrate-bearing sediments, JAPEX/JNOC/GSC Mallik 2L-38 gas hydrate research well by the Japanese research consortium; *in* Scientific Results from JAPEX/JNOC/GSC Mallik 2L-38 Gas Hydrate Research Well, Mackenzie Delta, Northwest Territories, Canada, (ed.) S.R. Dallimore, T. Uchida, and T.S. Collett; Geological Survey of Canada, Bulletin 544.

Walsh, J.B. and Brace, W.F.
1984:   The effect of pressure on porosity and the transport properties of rocks; Journal of Geophysical Research, v. 89, p. 9425–9431.

Washburn, E.W.
1921:   Note on a method of determining the distribution of pore sizes in a porous material; Proceedings of the National Academy of Science, v. 7, p. 115–116.

Winters, W.J., Dallimore, S.R., Collett, T.S., Katsube, T.J.,
Jenner, K.A., Cranston, R., Wright, J.F., Nixon, F.M., and Uchida, T.
1999:   Physical properties of sediments,from the JAPEX/JNOC/GSC Mallik 2L-38 gas hydrate research well; *in* Scientific Results from JAPEX/JNOC/GSC Mallik 2L-38 Gas Hydrate Research Well,

Mackenzie Delta, Northwest Territories, Canada, (ed.) S.R. Dallimore, T. Uchida, and T.S. Collett; Geological Survey of Canada, Bulletin 544.

Wright, J.F., Dallimore, S.R., and Nixon, F.M.,
1999:   Influences of grain size and salinity on pressure-temperature thresholds for methane hydrate stability in JAPEX/JNOC/ GSC Mallik 2L-38 gas hydrate research well sediments; *in* Scientific Results from JAPEX/JNOC/GSC Mallik 2L-38 Gas Hydrate Research Well, Mackenzie Delta, Northwest Territories, Canada, (ed.) S.R. Dallimore, T. Uchida, and T.S. Collett; Geological Survey of Canada, Bulletin 544.

APPENDIX A
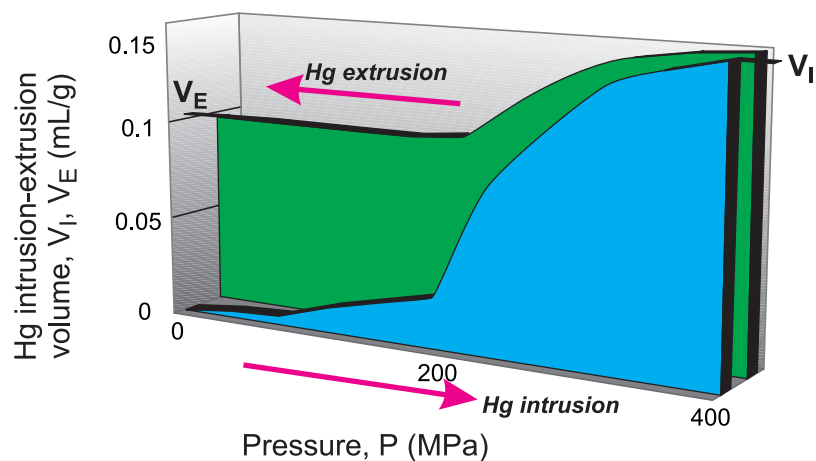
Figure A1. *Method for determining storage porosity ratio (ϕ_{rr}, Katsube et al., 1997). V_I=volume of Hg intruded, V_E=volume of residual Hg subsequent to extrusion.*